

<https://doi.org/10.1038/s44260-026-00076-0>

Multilayer networks characterize human-mobility patterns by industry sector for the 2021 Texas winter storm

Check for updates

Melissa Butler^{1,2}✉, Alisha Khan^{1,2}, Francis Osei Tutu Afrifa^{1,3}, Yingjie Hu⁴ & Dane Taylor^{1,2}✉

Understanding human mobility during disastrous events is crucial for emergency planning and disaster management. We develop a methodology to construct time-varying, multilayer networks where edges encode observed movements between spatial regions (census tracts) and network layers encode movement categories by industry sectors (e.g., schools, hospitals). Using the 2021 Texas winter storm as a case study, we find that people markedly reduced movements to ambulatory health care services, restaurants, and schools, but prioritized movements to grocery stores and gas stations. Additionally, we study the predictability of nodes' in- and out-degrees in the multilayer networks, which encode movements into and out of census tracts. Inward movements prove harder to predict than outward movements, especially during the storm. This case study highlights our methodology's effectiveness for detecting/characterizing mobility shifts, and our specific findings on the reduction, prioritization, and predictability of sector-specific movements aim to support mobility-related decisions during future extreme weather events.

Networks encoding the spatio-temporal patterns of human movements (i.e., mobility networks) have been developed and used to provide insights about daily commuting patterns^{1,2}, improve public transit infrastructures³, develop data-driven models for epidemic spreading^{4,5}, and reveal geographic insights about segregation⁶ and inequality⁷ (e.g., with respect to access to goods and services). Of note, multilayer networks^{8–10} have been adopted as a leading framework for mobility modeling, whereby different network layers have been utilized to represent different types of interconnected networks. Examples include networks that distinguish different modes of transportation^{11–13} or complementary infrastructures within a single mode of transportation (e.g., different airlines^{14,15}). Different layers can also be used to represent different sources of data for mobility¹⁶, and it's worth noting that one might expect each mobility network layer to adhere to different spatial and temporal constraints¹⁷.

In this work, we propose to study multilayer mobility networks in which different layers are defined according to the types of locations that persons visit—that is, the industry sector to which each location belongs. Different network layers are used, for example, to encode human movements to schools, grocery stores, hospitals, and so on. Our methodology involves studying observed movements using a cell-phone GPS dataset called SafeGraph¹⁸ and constructing multilayer networks that encode directed weekly flows between spatial regions. See Fig. 1 for an example

illustrating observed human movements from home neighborhoods to hospitals for Harris County, TX, during the week of a 2021 winter storm. Each network layer corresponds to an industry sector defined using the North American Industry Classification System (NAICS), which is a hierarchical classification scheme that gives rise to a hierarchy of network layers. This framework thereby allows for a rich, nuanced characterization, or “fingerprinting,” for human movements and movement changes and adaptations by industry sector that can occur, for example, seasonally or during disruptive events such as natural disasters. To illustrate this application, we apply this modeling framework to investigate how human mobility adapted during a winter storm. By studying how people adapt their movement patterns with respect to different categories of movement (e.g., visitations to schools, hospitals, and grocery stores), our approach examines ongoing and interrupted *local movements*. This provides complementary insights to prior research on different risk-aversion behaviors such as sheltering at home^{19,20} and large-scale evacuations^{21,22}—that latter of which is common for some disasters (e.g., earthquakes, hurricanes, and floods) but not winter storms²³.

Herein, we focus on human mobility adaptation during the 2021 Texas winter storm, or Winter Storm Uri, which hit Texas during February 13–17, 2021, and led to 246 deaths and more than \$195 billion damages²⁴. This extreme weather event caused a disruption in typical human mobility

¹School of Computing, University of Wyoming, Laramie, WY, USA. ²Department of Mathematics & Statistics, University of Wyoming, Laramie, WY, USA.

³Department of Atmospheric Science, University of Wyoming, Laramie, WY, USA. ⁴Department of Geography, University at Buffalo, Buffalo, NY, USA.

✉ e-mail: mbutle15@uwyo.edu; dane.taylor@uwyo.edu

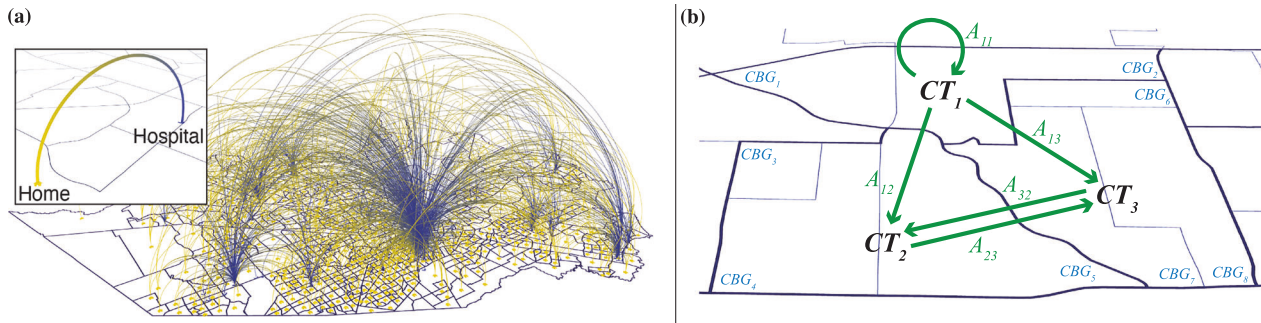


Fig. 1 | Networks summarize human movements between census tracts. **a** Visualization of observed movements from home neighborhoods to hospitals in Harris County, TX, during the storm week beginning on February 15, 2021 (Monday). Home locations are recorded using U.S. census block groups (which we enumerate CBG_i and which comprise larger spatial units called census tracts), whereas destination locations are points of interest (POIs) with known latitudes,

longitudes, and other information such as industry category (e.g., hospitals). **b** For different industry categories, we construct networks that are each encoded by a time-varying adjacency matrix in which $A_{ij}(t)$ encodes movements from one census tract to another, $CT_i \rightarrow CT_j$, where CT_i is a person’s home census tract, and they visit a POI in census tract CT_j during week t . We also study movements in and out of census tracts defined by their node degrees: $d_i^{in}(t) = \sum_j A_{ji}(t)$ and $d_i^{out}(t) = \sum_j A_{ij}(t)$.

patterns due to poor road conditions²⁵, the inability of people to leave their homes, government recommendations to stay home^{26,27}, and building closures²⁸. There was also a huge impact on key infrastructure, including water and power outages. Previous research on this event has focused on the state’s infrastructure, including the power grid²⁹, water infrastructure resilience³⁰, and social disparities during outages in these systems³¹. Other studies have used cell phone location data to examine the disproportionate impacts of this winter storm on different socioeconomic groups and community resilience^{32,33}.

Complementing these studies, our utilization of multilayer mobility networks provides a fine-grained characterization of the impacts of Winter Storm Uri on human movements to locations associated with different industry sectors. We first investigated which layers of the network were the most/least impacted by the storm, finding that people largely reduced their movements to ambulatory health care services, restaurants, and schools, but prioritized movements to grocery stores and gas stations. Much of our work focuses on understanding the network layers’ in- and out-degrees that encode the cumulative movements into and outward from census tracts (defined according to each industry sector). We integrate additional data from the U.S. Census, including demographic, socioeconomic, and infrastructure information, and train models for in- and out-degree predictions during the storm week and other weeks. We find that in-degrees are generally harder to predict than out-degrees, complementing known insights about the predictability of human movements^{34–36}. Interestingly, the predictability of out-degrees was not significantly impacted by the storm (with an R-squared score reduction of less than 1%), while the predictability of in-degrees decreased significantly during the storm week (with an R-squared score reduction of 4–13%).

Our work contributes to human behavior research during catastrophic events, aiming to obtain a deeper understanding of people’s adaptation and resilience to natural disasters by industry sector. Specifically, our work provides insights into which types of human movements are prioritized (e.g., those related to basic needs such as food, water, and shelter) and which are strategically reduced. Our findings about the predictability of movements into and out of census tracts can also aid emergency planning and disaster management for future extreme weather events. In short, our approach of using multilayer mobility networks to study the reduction, prioritization, and predictability of human movements categorized by industry sector broadens the understanding of how people adapt their mobility during situations of heightened risk.

Results

Multilayer networks encode human movements to different industry sectors

To develop a nuanced characterization of the storm’s impact on different categories of human movement, we first introduce a modeling

framework involving time-varying, multilayer networks. Different layers in the multilayer network represent observed movements associated with different industry sectors. Our study area is Harris County, TX, which was severely affected by the 2021 winter storm, and the study duration is 25 weeks beginning on Monday, December 28, 2020, and ending on Sunday, June 27, 2021. We enumerate these weeks $t = 1, \dots, 25$ and note that the storm’s most severe impacts occurred on February 15–17 during week 8. Following the literature^{32,37,38}, we aggregate census block groups and points of interest (POIs) across census tracts to yield networks that summarize observed movements from one census tract to another, and the movement destinations are associated with a particular industry category (e.g., hospitals). See Fig. 1 for a visualization and “Methods” for further details.

We construct different networks for different industry sectors, and we refer to the act of separating a network’s edges into categorized sets of edges associated with network layers as “stratification”³⁹. More specifically, we study a type of multilayer network called a multiplex network in which each layer consists of the same set of nodes (i.e., in our case, the set of census tracts) and, in our case, each layer encodes different behavioral categories of movement (e.g., visits to schools, hospitals, etc.). We classify behavioral categories of movement based on the 2017 NAICS, which were used to classify POIs in the SafeGraph data. Importantly, NAICS is a hierarchical categorization scheme, allowing us to stratify movement data into a hierarchical set of mobility network layers. Each NAICS category has a numerical code with two to six digits depending on level in the hierarchy, with two digits at the coarsest level and six digits at the finest, most-granular level. See Fig. 2a for a toy illustration of this hierarchy of network layers. For each NAICS code n , we define a time-varying adjacency matrix so that $A^{(n)}(t)$ describes network layer n during week t (see “Methods” for further details). In Fig. 2b, we depict a map of census tracts in Harris County TX, overlaid with visualizations of example network layers at three different levels of coarseness for the movement categories: all movements (top), movements to health care and social assistance locations (middle), and movements to hospitals (lower).

Our study will examine multilayer networks with layers associated with two hierarchy levels of categories. At the coarsest level, we focus on the eight industry categories with the highest movement: retail trade 1 (NAICS 44); retail trade 2 (45); real estate and rental and leasing (53); educational services (61); health care and social assistance (61); arts, entertainment, and recreation (71); accommodation and food services (72); and other services (81). See “Methods” for details on how we chose which categories to focus on. For the finer hierarchical level, we identified industry sectors according to the three-digit NAICS codes; however, for educational services (61), we used four-digit codes since the categories for 61 and 611 are identical.

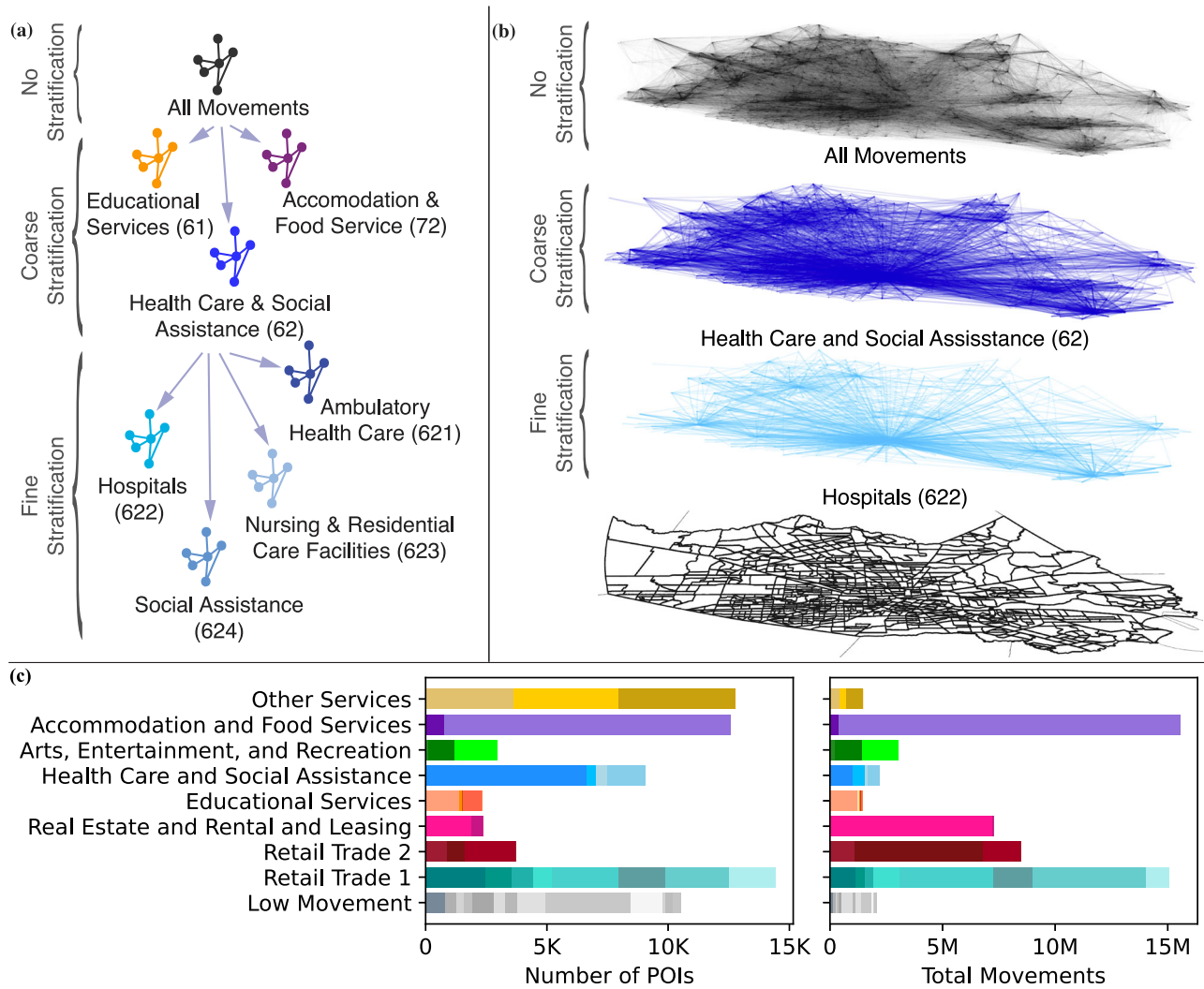


Fig. 2 | Hierarchical stratification of movement categories by industry sector. **a** Toy illustration for the hierarchical stratification of a mobility network into network layers that encode different behavioral categories of movements, defined using the North American Industry Classification System (NAICS). The number of digits in a NAICS code determines the hierarchy depth (i.e., level of coarseness when refining movement categories into subcategories). **b** A map of census tracts in Harris County (bottom) overlaid by three example networks at three different coarseness

levels: all movements (top), health care and social assistance (middle), and hospitals (lower). **c** Fraction of POIs in each NAICS category for Harris County (left) and fraction of total observed movements in each NAICS category (right). In both panels, for each category, different coloration indicates finer subcategories. See Fig. 4 and Supplementary Fig. 1 for additional details about the stratification of categories into subcategories and their industry sector NAICS codes.

Movements significantly decreased during the storm week

Using multilayer networks encoding high-movement industry categories, we study their structure to investigate the impact of the storm on human behavior. Our approach relies on statistical analyses of the node degrees for the network layers and the “aggregated network” that does not distinguish movement categories. Beginning with the coarsest level of movement categorization (i.e., two-digit NAICS codes), for each n we examined the time series $m^{(n)}(t) = \sum_{i,j} A_{ij}^{(n)}(t)$ of total movements for a 25-week study duration from December 29, 2021 to June 28, 2021 and computed z-scores $Z^{(n)}(t)$ (see “Methods”) to identify statistically significant differences between $m^{(n)}(t)$ and baseline values that were found using the 6 weeks preceding the storm.

A visualization of this calculation is provided in Fig. 3a for an example network layer encoding movements to locations associated with health care and social assistance (i.e., NAICS code 62). We find $Z^{(62)}(8) \approx -27$, implying that these movements significantly decreased during the storm, i.e., by approximately 27 standard deviations. In Fig. 3b, we plot z-scores $Z^{(n)}(t)$ for the high-movement categories across the 25-week study duration. Observe that all of the coarse-level categories of movement that we considered

exhibited a decrease during the storm week ($t = 8$). The most impacted movement categories are health care and social assistance (62), accommodation and food services (72), and educational services (61). Movements in these categories are significantly reduced, which is likely due to the closures of hospitals, schools, and restaurants during the storm. In contrast, retail trade 1 (44), which includes grocery stores and other essential food vendors, appears to have been the least affected. Movements to these locations were prioritized despite the heightened risk imposed by the storm. For the weeks following the storm, movements increased across all categories, which is aligned with a seasonal trend that occurs each spring. See Supplementary Fig. 2 for a multi-year time series showing this trend across movement categories.

Before continuing, we highlight that the storm’s impact appears to occur exclusively during week 8 (February 15–21, 2021), which is expected since the most severe effects (e.g., blackouts and deaths) occurred on February 15–17. It’s worth pointing out that the network data is aggregated across a larger time window (i.e., the full week), but the anomalous storm largely caused network structural changes primarily during a subset of those days. Aggregating temporal network data across a larger time window is

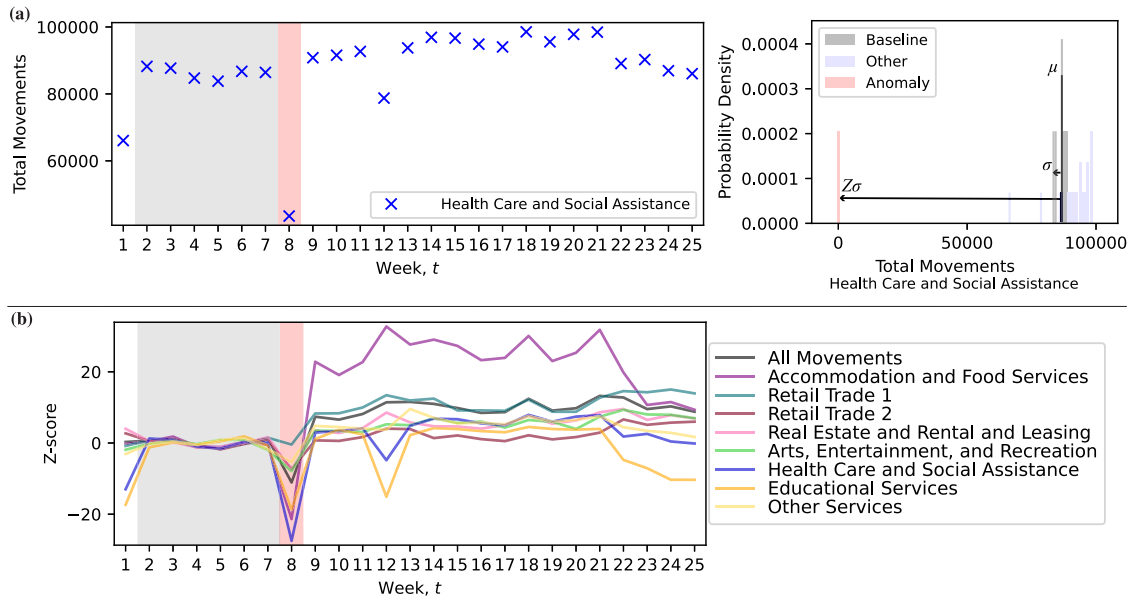


Fig. 3 | Decreased movement during storm, quantified by z-scores. a We plot the total movements $m^{(n)}(t) = \sum_{i,j} A_{ij}^{(n)}(t)$ during each week t for the network layer that encodes observed movements to locations associated with health care and social assistance (NAICS code 62). Red and gray shading highlight the storm week and the weeks used to construct a baseline for comparison. We quantify the change in

movements during the storm week, $t = 8$, using a z-score $Z^{(n)}(t) \approx -27$, which is visualized in the right-hand panel and is discussed in “Methods.” Its calculation uses a baseline mean, $\mu^{(n)}$, and standard deviation, $\sigma^{(n)}$. **b** We plot the z-scores, $Z^{(n)}(t)$, versus t for the eight NAICS categories with the largest total movements across the 25-week study duration.

known to cause network properties to have diminished signal strengths^{40,41}. Here, we expect that the z-scores would generally increase (i.e., enhanced signal detection) if we were able to select a time window to perfectly align with the storm days. However, the dataset we study is provided at the weekly timescale; nevertheless, the anomaly signal is very strong.

That said, there are several other anomalous decreases in movement for some categories. Week 1 includes the holiday of New Years, and we observe that this week has decreased movement to locations associated with health care (62), education (61), and other services (81) but increased movement to locations associated with real estate (53) and retail trade 2 (45). In addition, decreased movements to health care and education facilities occur during week 12, which we predict occurs due to the school closures and increased vacationing that occurs during spring break. Finally, starting week 22, we observe decreased movement to educational facilities, which likely occurs due to the start of summer break.

We also note that our baseline weeks coincide with the end of the COVID-19 period⁴² and acknowledge the difficulty to disentangle the lingering effects of the pandemic from the storm. In Supplementary Fig. 2, we see for our study duration that the majority of movement categories had returned to their pre-pandemic numbers, with the exception of educational services, health care, and accommodation (which could be considered the new normal movement patterns).

Storm impact on movements with a finer stratification of industry sectors

So far, we have only considered movement categories (i.e., network layers) defined at a coarse scale in which the mobility network is stratified into coarsely defined movement categories using two-digit NAICS codes. However, NAICS is a hierarchical classification scheme allowing us to stratify movement categories (and their associated network layers) into a hierarchy. Next, we extend our study of z-scores by considering a finer stratification of movement categories using three-digit NAICS codes (except for educational services, for which we used four digits, since using three digits does not provide a finer stratification).

In Fig. 4, we visualize the z-scores during the storm week for a coarse stratification of movement categories on the left and a finer stratification on the right. Both sets of NAICS codes (i.e., coarse versus fine) are ordered from

top-to-bottom in order of z-score so that the most decreased movement categories are at the top. Curved lines show how each coarse movement category separates into finer categories, and the line widths are proportional to the total movement for each category. We also note that the category containing business schools and computer and management training (6114) is omitted due to the observed movements being too small (i.e., only two were observed).

We first highlight that there is remarkable consistency between the three most-impacted movement categories at the coarse scale and at the fine scale. The three most-impacted coarse movement categories were (62) health care, (72) accommodation and food services, and (61) education. At the finer scale, the 3 most-impacted subcategories are derived from these 3 categories, one each, and their z-scores retain the same order. The most impacted fine-scale movement category is ambulatory health services, $Z^{(621)}(8) = -34.49$, which includes POIs such as physician and dentist offices, outpatient care centers, and home health care services. The second is food service and drinking places, $Z^{(722)}(8) = -22.18$, and further examination revealed that restaurants is most impacted sub-sub-category (i.e., $Z^{(7225)}(8) = -21.37$). (We must note that the COVID-19 restriction on restaurant capacity in Harris County had been at 50% during the storm week and was only raised back to 100% on March 10, 2021⁴³.) Lastly, movements to elementary schools is the third most-impacted fine-scale category, $Z^{(6111)}(8) = -19.34$, while other educational institutes like universities and junior colleges were less impacted.

Importantly, Fig. 4 also reveals which categories of movement were prioritized during the storm. Movements to food and beverage stores (445) decreased very little, and at the same time, movements actually increased to three types of locations: gasoline stations, $Z^{(447)}(8) = 8.89$ (which are critical infrastructure and offer easily accessible food), accommodations, $Z^{(721)}(8) = 4.13$ (which includes hotels for dislocated peoples but also has a regular seasonal increase shown in Supplementary Fig. 2), and building materials, $Z^{(444)}(8) = 4.07$ (which includes home stores including Home Depot and Lowes).

Storm impact on mobility networks’ in- and out-degrees

In this section, we study the in-degree $d_j^{in}(t)$ and out-degree $d_j^{out}(t)$ that encode the weekly movements into and out of, respectively, each census

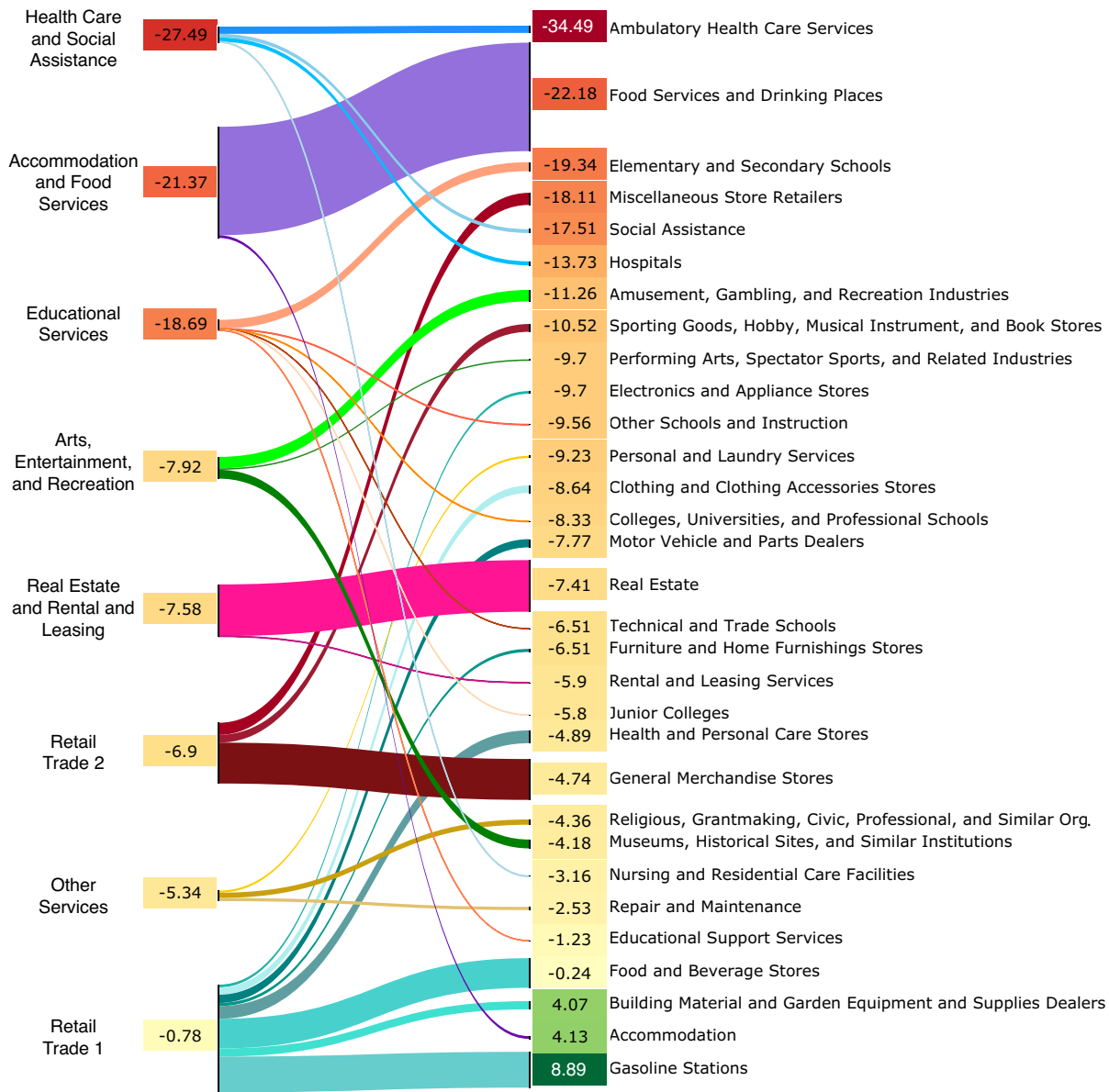


Fig. 4 | Comparing the storm’s impact on movement categories and sub-categories. Z-scores quantify the storm’s impact on movement categories defined using the NAICS hierarchical classification scheme. These are shown using both a coarse scale with two-digit NAICS codes (left) and a finer scale using three or four-digit NAICS codes (right). See Supplementary Fig. 1 for the industry sector NAICS

codes. Both sets of movement categories are ordered top-to-bottom based on their computed z-scores (shown in colored boxes), so the most-decreased movement categories are at the top. Curved lines depict how coarse movement categories separate into finer categories, and the line widths are proportional to the number of observed movements for each category.

tract CT_j . We note that we study “weighted degrees” (which are also commonly called node “strengths”). In Fig. 5a, we show distributions of in- and out-degrees during the storm week (red) and during the six baseline weeks preceding the storm (blue). These distributions were computed across the 786 census tracts in Harris County using 10 bins. Observe that both degree distributions appear linear in a log-log scale, which suggests a power-law relation (although there is limited evidence, since the degree heterogeneity spans only about 1.5 decades). Because network connectivity decreases during the storm, the node degrees decrease during the storm, which manifests as a shift-left for the degree distributions. Interestingly, the degree distributions do not otherwise significantly change. In Fig. 5b, we show that similar degree distributions arise for the network layers that encode different movement categories, and they are similarly impacted by the storm.

To help understand the origin (or main drivers) of degree heterogeneity across census tracts, next we support two hypotheses: *census tracts with large (or small) populations should have many (or few) outward*

movements; and census tracts containing many (or few) POIs should have many (or few) inward movements. Thus motivated, in Fig. 5c, we plot (left) $d_i^{out}(t)$ versus census tract population size and (right) $d_i^{in}(t)$ versus the number of POIs, respectively, for the census tracts in Harris County. Both pairs of variables exhibit significant correlation with Pearson correlation coefficients given by $r \approx 0.85$ and $r \approx 0.66$, respectively, with p values within numerical precision of zero.

Next, we extend this correlation study to the network layers that encode different movement categories. That is, for each network layer associated with each NAICS code n , we calculate each CT_j ’s out-degree $d_i^{out,(n)}(t) = \sum_j A_{ij}^{(n)}(t)$ and in-degree $d_i^{in,(n)}(t) = \sum_j A_{ji}^{(n)}(t)$ and then calculate the associated Pearson correlation coefficients r comparing these degrees to a census tract’s population and related infrastructure (i.e., the number of POIs in that census tract having that particular NAICS code n). The associated r values across baseline weeks are reported in Fig. 5d. For comparison, we also include correlations between out-degree vs. number of

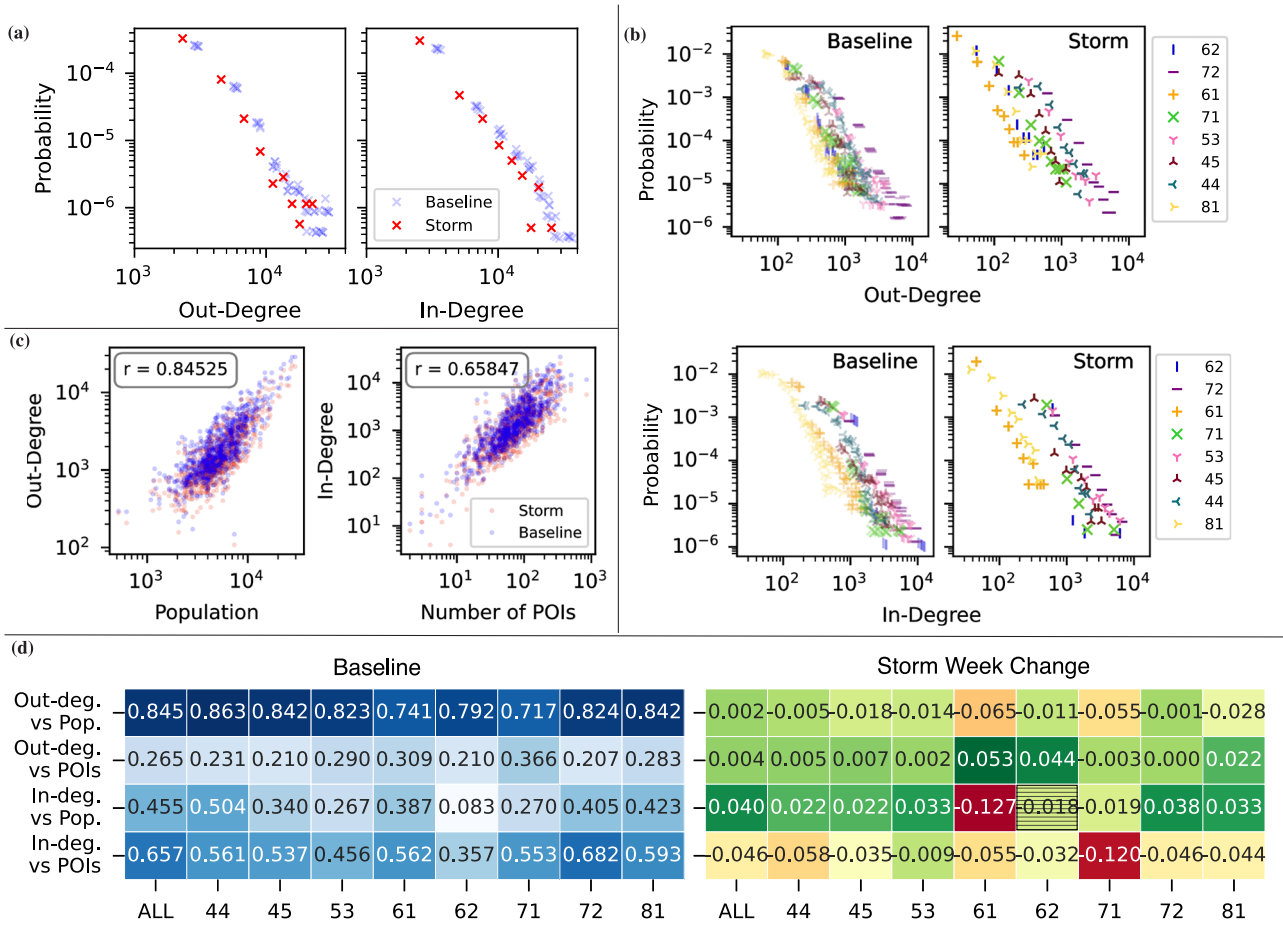


Fig. 5 | Node degrees reveal heterogeneous flows among census tracts. **a** We show distributions of in-degrees $d_i^{in}(t)$ and out-degrees $d_i^{out}(t)$ for the mobility network combining all movement categories (left) during the six baseline weeks (blue) and storm week (red). **b** Focusing on network layers associated with high-movement categories, we plot the distributions of in- and out-degrees for both the baseline weeks and the storm week. The probabilities decay linearly on a log-log scale, suggesting a power-law relation. **c** Scatter plots reveal that (left) a census tract’s out-degree is strongly correlated with the population residing in that census tract, and

(right) a census tract’s in-degrees is strongly correlated with its infrastructure (i.e., the number of POIs in the census tract). **d** For high-movement categories during the baseline weeks, Pearson correlation coefficients (r values) measure correlation between census tracts’ in- and out-degrees versus their populations and the number of POIs for each industry sector. We report how the r values changed during the storm week (i.e., r for storm week minus s for the baseline weeks). (We note that all p values were smaller than 0.05 except for one instance, which is outlined by a black box.)

POIs and in-degree vs. population. In Fig. 5d, we show how each Pearson correlation coefficient changed during the storm week (right). Note that all correlations are statistically significant with p values below 0.05, except for the one value that is highlighted by a black box (see NAICS 62 for the storm week).

Observe in Fig. 5d that the strongest correlation occurs between out-degrees and census tract populations with $r \in [0.71, 0.87]$ across all movement categories. The second-strongest correlation occurs between in-degrees and the numbers of POIs in census tracts, with $r \in [0.35, 0.69]$ across all movement categories. We additionally observe a correlation between out-degrees and POI numbers, and between in-degrees and population; however, their associated r values are generally smaller. Similar to our hypothesis for Fig. 5c, this suggests that even at the resolution of individual movement categories, population drives outbound movement, while local infrastructure attracts inbound visits. We also do not find much variation across different movement categories, with the exception of movement category health care and social services (62), which has lower r values for correlations relating to in-degrees. We predict this lower correlation occurs due to the nature of hospital infrastructure, i.e., fewer hospitals exist, and each serves as a centralized hub that attracts large numbers of visitors. Turning our attention to the storm week, we find that the storm’s effect on correlations is small. The largest changes to r occur for the correlation

between in-degree and population for educational services (61) and between in-degree and POI numbers for arts and entertainment (71).

Predictability of node degrees using demographic, socio-economic, and infrastructure information

In the previous section, we supported our hypothesis that census tract population is a main driver for outward movements, while POI infrastructure is a main driver for movements into census tracts. We now use multivariate linear regression to perform a broader investigation of how network connectivity during normal times and the storm week are associated with demographic, socioeconomic, and infrastructure information. That is, we obtain predictive models for census tracts’ in- and out-degrees using infrastructure variables (i.e., the number of POIs in each census tract) and six social factors from U.S. Census data: population, population density, income, non-white percentage, poverty rate, and unemployment rate. See “Methods” for discussions on the dataset, this modeling framework, and our use of variance inflation factors to select a subset of social factors while preventing variable multicollinearity. To prevent multicollinearity for the infrastructure information, we use either the total count of POIs across NAICS categories or separate counts for the different NAICS categories. We restrict our models to the eight NAICS categories associated with the most movement (see Fig. 2c).

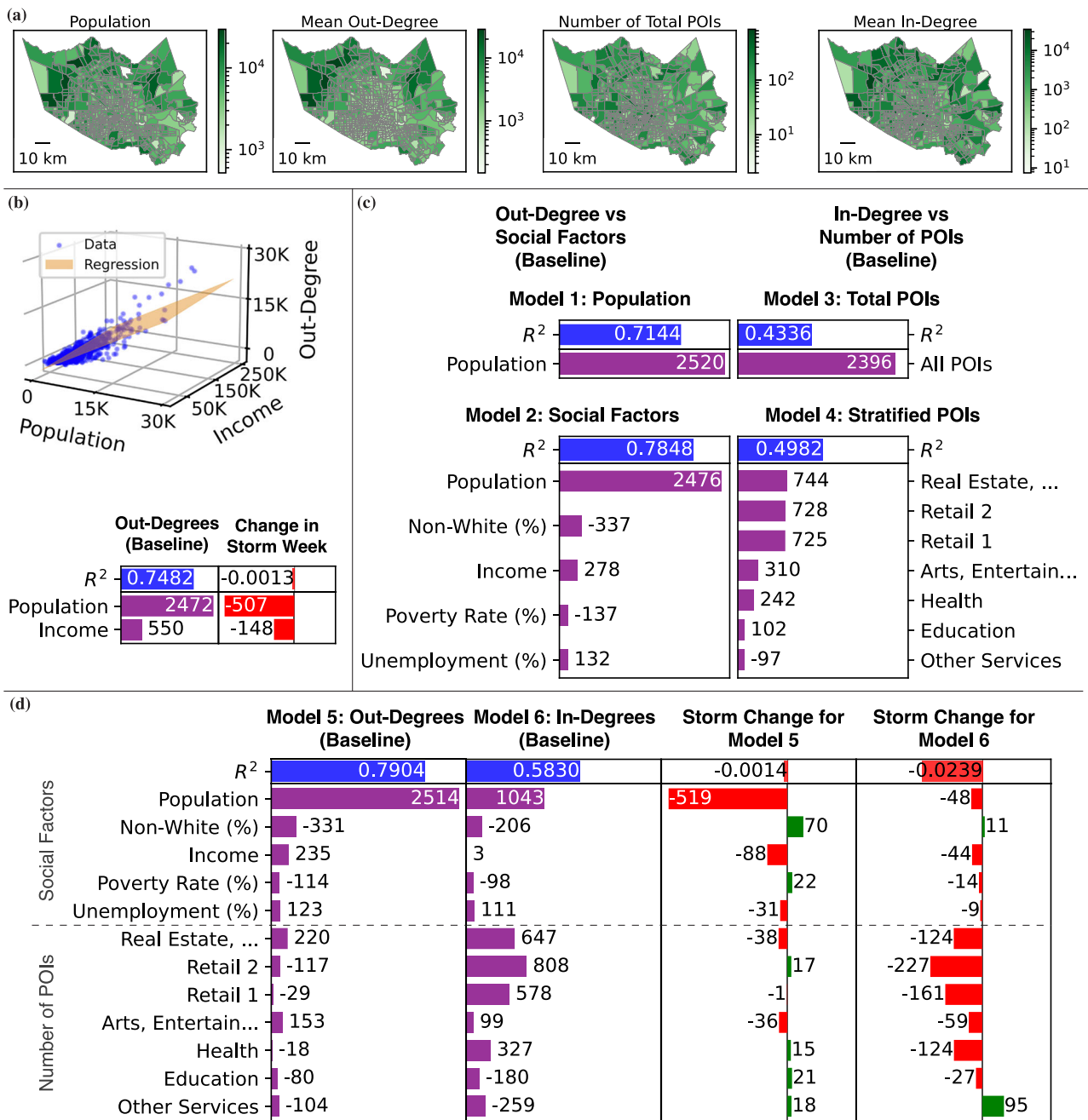


Fig. 6 | Multivariate linear regression for predicting inward and outward movements. **a** Choropleth maps of census tract’s in Harris County, TX are used to visualize two key regression features (populations and the number of total POIs in census tracts) and the two target variables (in- and out-degree). We note that our analysis omits census tract 980000, for which the population and number of POIs is unusually small (i.e., 4 and 1, respectively), and we have colored that census tract gray. **b** Visualization of a multivariate linear regression model that predicts out-degrees based on two input features (population and income) and takes the geometric form of a two-dimensional plane that is fitted to empirical observations.

(Each data point represents a census tract in Harris County.) We additionally provide the model’s R^2 -score, that measure prediction accuracy, as well as its regression coefficients. It is also indicated how the model changes when fit to data during the storm week. **c** We report R^2 and regression coefficients for four additional regression models that predict either out-degrees versus social factors (models 1 and 2) or in-degrees versus number of POIs (models 3 and 4). **d** Similar information is given for models 5 and 6 that use all input features. It is also indicated how these models change when fit to data during the storm week.

In Fig. 6a, we depict choropleth maps for Harris County that visualize two key features for the regression models: population and the number of total POIs in each census tract. We additionally visualize the census tract’s mean out- and in-degrees across the baseline weeks. In Fig. 6b, we provide a visualization to illustrate our multivariate regression analysis that predicts census tracts’ out-degrees using two social factors (population and income) and no infrastructure information. In the top panel, we illustrate the two-dimensional regression plane (yellow) and the observed values across census

tracts (blue). In the bottom, we quantify prediction accuracy using R^2 -scores, which in this case is given by $R^2 \approx 0.748$. Note this prediction accuracy outperforms linear regression using just census tract population, since for single-variable regression the R^2 -score is given by the square of the Pearson correlation coefficient: $R^2 \approx 0.84525^2 \approx 0.714$. That is, including income (i.e., as well as population) yields a 4.7% accuracy improvement for predicting movements outward from census tracts. We provide bar graphs that summarize R^2 and the regression coefficients (left).

Note the coefficient for population is much larger than that for income, highlighting that population is the more-important social factor for out-degree predictions. The bar graph on the right indicates how R^2 and the regression coefficients change if the regression model is fit to data restricted to the storm week; R^2 changes minimally, but the coefficients decrease by 20–26%.

In Fig. 6c, we report R^2 and regression coefficients for several regression models. In models 1 and 2, we study how movements outward from census tracts are related to social factors. That is, we constructed two regression models that predict out-degrees using either: only population (model 1) or all six social factors (model 2). Comparing the two models, observe that including the five additional social factors increases R^2 by 9.85% (i.e., from 0.714 to 0.784). Also note that the largest regression coefficients (in order) are population, population density, non-white percentage, and income. That is, we find these to be the most important census tract variables for predicting movements outward from census tracts. For models 3 and 4, we study how movements into census tracts are related to industry information, i.e., the number of POIs. We predict in-degrees using either: total POI counts, while ignoring NAICS codes (model 3), or stratified POI counts for different NAICS codes (model 4). Comparing models, observe that R^2 increases 14.9% when POI counts are calculated separately for the different NAICS codes, and the most important codes (in order) are 53, 45, 44, and 72. Interestingly, these are the four NAICS categories associated with the highest movements (recall Fig. 2c).

In Fig. 6d, we study how movements outward and inward to census tracts are related to all features (social factors and industry information) for the baseline weeks (models 5 and 6) and the storm week. Comparing model 5 (predicting out-degrees using all features) to model 2, observe that R^2 has a very modest 0.71% increase and that the regression coefficients associated with POI counts are relatively small. Similarly, comparing model 6 (predicting in-degrees using all features) to model 4, observe that R^2 increases by a significant 17%, and population has a very large regression coefficient (with the other coefficients for social factors being small). Finally, in the last two columns of Fig. 6d, we report how R^2 and the regression coefficients changed when the multivariate regression models were fit to the data during the storm week. We first consider the models that predict out-degrees during the storm (change for model 5), finding that the models' regression coefficients significantly change (almost always decreasing in magnitude); however, R^2 changed by less than 1%. That is, outward movements can be predicted with nearly the same accuracy during the storm week. We next consider the models that predict in-degrees during the storm (change for model 6), for which R^2 decreased by 4%, and we see a decrease in the importance of industry information. Lastly, while not included in the table, we also studied how the models 1–4 changed during the storm week. We found that during the storm, R^2 dropped by less than 1% when predicting out-degree vs social factors, but that they dropped by 12–13% when predicting in-degree vs number of POIs.

In conclusion, inward movements into census tracts are generally harder to predict than outward movements (e.g., R^2 are much smaller for in-degree versus out-degree), and their prediction is also much more impacted by the storm (e.g., the drop in R^2 is much greater).

Discussion

In this work, we studied human mobility using time-varying, multilayer networks in which edges encode observed movements between spatial regions (i.e., census tracts) and network layers encode different movement categories that were defined according to industry sector (e.g., visitations to schools, hospitals, and grocery stores). While multilayer networks were utilized to encode different modes of transportation (e.g., roadways versus metro lines) in previous human mobility research^{11–13}, our study leveraged them to encode different industry sectors of movements and investigated human mobility changes in different layers during a major disaster: Winter Storm Uri. By considering mobility patterns by industry sector, we gained complementary insight about how the same storm can have different impacts on human movements in different industry sectors.

Focusing on Harris County, TX, we found that people reduced their movements to ambulatory health care services, restaurants, and schools, but prioritized movements to grocery stores and gas stations. We additionally studied the predictability of inward and outward movements for census tracts using information about their demographic, socioeconomic, and infrastructure characteristics. We found that, as compared to outward movements (i.e., out-degrees), inward movements (i.e., in-degrees) are harder to predict, especially during the storm. These insights into the reduction, prioritization, and predictability of human movements during Winter Storm Uri could be useful for supporting the decisions of policy-makers and emergency responders during extreme weather events.

More broadly, this case study illustrates the effectiveness of our methodology for detecting and characterizing mobility shifts, suggesting that it will be useful for diverse scenarios even beyond weather events. It is also worth noting that the mobility changes observed herein reflect a combination of influences, including voluntary choices, power outages, and government edicts (e.g., building closures and travel recommendations). While we cannot decouple these effects for Storm Uri, our techniques should be useful for diverse scenarios, including those with or without top-down directives from government officials. Moreover, it is interesting to consider whether it is even possible, in principle, to disentangle these various drivers for human-movement change. If so, stratifying mobility networks by industry type (as we have proposed) could lead to fruitful directions to address this open challenge.

We end by highlighting a few additional future directions for research. In this paper, we constructed network models in which weighted edges encode the numbers of observed movements, and it would be interesting to study other types of networks, including those where edge weights are normalized (e.g., by the density of devices) or reflect geospatial information (e.g., distances between census tracts, census tract land areas, and spatial partitioning biases). We also studied a set of social factors that did not include age-related information (i.e., which were removed during variance inflation factor tests to remove correlated drivers and ensure statistical rigor as discussed in “Methods”) and it would be interesting to investigate how different age groups were impacted in future research. However, it is also known that mobile-device data underrepresent older populations^{44,45}, posing a major challenge to such a study. One could also broaden the characterization of the anomalous week by using quantification methods besides z -scores and by considering different choices for selecting baselines that incorporate, e.g., seasonal and annual trends. Incorporating data from multiple years is another direction; the 2020 data is significantly impacted by COVID-19, but one could explore techniques to debias its impacts. Also, it would be interesting to compare our retrospective study of human mobility during Winter Storm Uri to movements observed in other extreme weather events. Finally, further study of the predictability of specific industry categories would benefit the understanding of the increased demand on certain industries as well as provide insight into the varied predictability of different categories.

Methods

Construction of multilayer networks

We study a dataset of weekly human movements from the data provider SafeGraph. The approximately 700 GB dataset is collected based on the GPS locations of opt-in smart mobile devices (mostly smartphones), and captures weekly movements of people from a home location, recorded at the corresponding census block group, to a destination location, i.e., a specific POI. We use the Python library *safegraph_py* to process and prepare the data into this graph-structured format, and computations were implemented on the NCAR-Wyoming Supercomputing Center.

The original SafeGraph data can be encoded by a time-varying, bipartite graph $G(t)$, for $t = 1, \dots, T$, where T is the total number of weeks studied. Each graph $G(t)$ is composed of weighted, directed edges that encode the number of observed movements between a source census block group and a destination POI. We denote $\mathcal{H} = \{\text{CBG}_i\}_{i=1}^H$ to be a set of source nodes (i.e., the home census block groups associated with mobile

devices), where H is the total number of census block groups in the studied area, and let $\mathcal{P} = \{\text{POI}_i\}_{i=1}^P$ be a set of destination nodes (i.e., the set of POIs), where P is the total number of POIs. POIs are identified using SafeGraph’s Placemeter system, a universal location identifier that combines a geospatial encoding system with a unique POI identifier that provides information including the name, latitude and longitude, business details, and industry classification. For privacy reasons, SafeGraph omits sparse data in which fewer than four visitors are recorded in a given week from any home census block group to a POI. Each edge (i, j) in $G(t)$ has a weight $B_{ij}(t)$ that encodes the number of observed movements from census block group CBG_i to point of interest POI_j during week t . Equivalently, each graph $G(t)$ can be encoded by a weighted adjacency matrix, $B(t) \in \mathbb{R}^{H \times P}$.

We first discuss the coarse-graining of SafeGraph data to the spatial resolution of census tracts. We define $\mathcal{C} = \{\text{CT}_i\}_{i=1}^C$ to be a set of census tracts of interest, where C is the total number of census tracts ($C = 786$ for Harris County), and let \mathcal{H}_i and \mathcal{P}_i denote, respectively, the census block groups and POIs within census tract CT_i . Then the combined observed movement from census block groups in census tract CT_i to POIs in census tract CT_j during week t is given by

$$A_{ij}(t) = \sum_{i' \in \mathcal{H}_i, j' \in \mathcal{P}_j} B_{i'j'}(t). \tag{1}$$

The remainder of this study examines time-varying networks encoded by square adjacency matrices $A(t)$ that are size $C \times C$. Finally, for each network, we define $d_i^{\text{out}}(t) = \sum_j A_{ij}(t)$ to be the out-degree—that is, a measure for all movements during week t that leave census tract CT_i —and $d_i^{\text{in}}(t) = \sum_j A_{ji}(t)$ to be the in-degree—that is, a measure for all movements to POIs within census tract CT_j during week t . For the mobility network in Fig. 1b, for example, in- and out-degrees for census tract CT_1 would be $d_1^{\text{in}}(t) = A_{11}(t)$ and $d_1^{\text{out}}(t) = A_{11}(t) + A_{12}(t) + A_{13}(t)$.

We next discuss behavioral stratification of the networks into different layers that encode movements to POIs that are associated with different industry categories based on the NAICS hierarchy. Letting \mathcal{N} denote the set of NAICS codes with a fixed number of digits, for each $n \in \mathcal{N}$ we define $\mathcal{P}_j^{(n)}$ as the set of POIs within census tract CT_j having NAICS code n . The network layers’ adjacency matrices are then obtained by $A_{ij}^{(n)}(t) = \sum_{i' \in \mathcal{H}_i, j' \in \mathcal{P}_j^{(n)}} B_{i'j'}(t)$. For each network layer n and census tract CT_i , we define the time-varying in- and out-degrees by $d_i^{\text{in},(n)}(t) = \sum_j A_{ji}^{(n)}(t)$ and $d_i^{\text{out},(n)}(t) = \sum_j A_{ij}^{(n)}(t)$, respectively. Finally, note that summing $A_{ij}^{(n)}(t)$ over all possible $n \in \mathcal{N}$ recovers the adjacency matrix $\sum_n A^{(n)}(t) = A(t)$ of the original, non-stratified network (i.e., also called the layer-aggregated network). One can similarly obtain the in- and out-degrees for the network encoding all movements by summing over the network layers: $d_i^{\text{in}}(t) = \sum_n d_i^{\text{in},(n)}(t)$ and $d_i^{\text{out}}(t) = \sum_n d_i^{\text{out},(n)}(t)$.

Determining threshold for high-movement categories

For many of the NAICS categories, the number of observed movements can be much smaller than that for other categories. Therefore, throughout this paper, we will often focus on the categories with the most movements. In Fig. 2c, we show the number of POIs by NAICS category for Harris County (left), $\sum_j |\mathcal{P}_j^{(n)}|$, whereas in Fig. 2c we depict the total movements for each category (right). That is, for each NAICS code $n \in \mathcal{N}$, we compute $m^{(n)}(t) = \sum_{i,j} A_{ij}^{(n)}(t)$ to be the total movement during week t and $M^{(n)} = \sum_t m^{(n)}(t)$ to be the total movement across the study duration. The coloration in each bar depicts the finer subcategories (i.e., NAICS codes with three to four digits). We then divide the two-digit NAICS categories into a set $\mathcal{N}_{\text{high}} = \{n | M^{(n)} \geq 10^{-6}\} = \{44, 45, 53, 61, 62, 71, 72\}$ of high-movement categories and a set $\mathcal{N}_{\text{low}} = \{n | M^{(n)} < 10^{-6}\}$ of low-movement categories. The choice of 10^{-6} was selected as a natural

partition of the dataset, since the total movements are much larger for educational services versus transportation services (i.e., $M^{(61)} = 1,462,340$ versus $M^{(48)} = 475,732$), which is the largest percentage change. The $M^{(n)}$ values of all two-digit NAICS categories and a detailed breakdown of the categories into subcategories are shown in Supplementary Table 1. This provides an overview of the hierarchy of layers and the total amount of movement in each layer for Harris County. The set \mathcal{N}_{low} contains 16 categories and are either combined into a “low-movement category” or omitted from our study.

Z-scores quantify movement-change significance

We quantify the storm’s impact on total movements for different network layers by comparing the total movements $m^{(n)}(t)$ during the storm week to a baseline of weekly movement, and we use z-scores to measure deviation from typical behavior. We apply this approach to different network layers to identify which movement categories undergo statistically significant change. After visually inspecting time series encoding weekly movements for several years of data (see Supplementary Fig. 2), we select the baseline that consists of the six weeks prior to the storm, $\mathcal{T}_{\text{base}} = \{2, 3, \dots, 7\}$. Letting μ and σ denote the mean and standard deviation of $m(t)$ across $t \in \mathcal{T}_{\text{base}}$, we compute the z-score $Z(t) = \frac{m(t) - \mu}{\sigma}$ to study the storm’s impact on all movement categories. Similarly, for each movement category n , we let $\mu^{(n)}$ and $\sigma^{(n)}$ denote the mean and standard deviation of $m^{(n)}(t)$ across $t \in \mathcal{T}_{\text{base}}$ and compute the z-score

$$Z^{(n)}(t) = \frac{m^{(n)}(t) - \mu^{(n)}}{\sigma^{(n)}}. \tag{2}$$

We compare z-scores across movement categories in Results.

Regression analysis relates movements to infrastructure, demographic, and socioeconomic information

In “Results,” we study the in- and out-degrees for network layers and investigate how these structural properties relate to infrastructure information (i.e., derived from the POIs) as well as social factors, including demographic and socioeconomic information. To this end, we gathered data from the U.S. Census Bureau, accessing tables from the 2010 American Community Survey and filtering for the year 2019 and census tracts in Harris County, TX. For each census tract, we assembled data for 13 social factors: population (B01003), population density, under 18 (DP05), under 5 (DP05), income (B19013), unemployment (DP03), poverty rate (S0601), non-white percentage (B02001), non-hispanic and non-black percentage (S0601), owner occupied percentage (B25003), renter occupied percentage (B25003), education level (S0601).

To identify which social factors have the strongest correlation with the networks’ in- and out-degrees, we conduct a multivariate linear regression. Noting that some social factors are correlated, provide redundant information, and cause regression instability, we sought to obtain a smaller set of social factors. Specifically, we conducted variance inflation factor (VIF) tests to identify and remove variables that are multicollinear, which can distort regression coefficients and reduce the model’s reliability. For each social factor, $X^{(i)} \in \mathbb{R}^{786}$, $i = 1, \dots, 13$, we calculated $\text{VIF}_i = 1/(1 - R_i^2)$, where

$$R_i^2 = 1 - \frac{\text{residual sum of squares}}{\text{total sum of squares}} = 1 - \frac{\sum_{j=1}^{786} (X_j^{(i)} - \hat{X}_j^{(i)})^2}{\sum_{j=1}^{786} (X_j^{(i)} - \bar{X}^{(i)})^2}, \tag{3}$$

R_i^2 is called the coefficient of determination. Here, each $\hat{X}^{(i)}$ is a predicted value from regression, and $\bar{X}^{(i)}$ is the mean across observed values.

In Table 1, we summarize our results for several VIF tests that were run using the *statsmodels* module in Python. For Test 1, we used 12 predictors that span three categories: demographic, socioeconomic, and race/ethnicity. In Test 2, we removed a predictor from each category, which were selected based on having a high VIF value in Test 1. For Test 3, we removed two

Table 1 | Variance inflation factor (VIF) tests to identify and remove variables with multicollinearity

Category	Predictor	Test 1	Test 2	Test 3	Test 4
Demographic	Population	5.318	4.785	3.531	3.375
	Population Density	3.308	3.292	2.687	2.672
	65 years and over (%)	8.458	5.516	5.444	–
	Under 18 (%)	84.755	–	–	–
Socioeconomic	Income	14.488	6.156	5.177	2.675
	School Enrollment (%)	63.847	12.666	–	–
	Unemployment (%)	4.884	4.814	4.535	4.255
	Poverty Rate (%)	8.111	7.557	4.021	3.933
	Renter Occupied (%)	18.919	8.367	–	–
	Owner Occupied (%)	28.744	–	–	–
Race/Ethnicity	Non-White (%)	6.201	5.609	5.038	4.849
	Non-Hispanic and Non-Black (%)	10.992	–	–	–

For Test 1, we used 12 predictors from three categories, resulting in most VIF values being greater than 5 (which is a standard threshold). Then we conducted successive tests to remove the highest VIF score from each category (while leaving at least one per category). For the final test (Test 4), each predictor in Test 3 was removed one at a time to identify a set of factors such that no VIF values were greater than 5.

predictors with the highest VIF values from Test 2. Finally, Test 4 showed that the VIF values of all remaining predictors were less than 5 (which is a standard threshold in VIF tests). The final six predictors are: population, population density, income, unemployment %, poverty rate %, and non-white %.

In addition to the social features above, we also include infrastructure features for each census tract in the form of the number of POIs. We look at the total number of POIs for each census tract as well as a breakdown of the number of POIs for the high-movement categories, $\mathcal{N}_{\text{high}}$, shown in Fig. 2c. We highlight that we never include both the total number of POIs and the stratified POIs into categories, since that would introduce collinearity into the model (i.e., the total of POIs equals the summation over POIs in different categories). Each model defines a relationship between either in- or out-degrees and a set of features, $\{X^{(i)} | i \in S\}$, where S is a set of select indexed features (possibly including demographic, socioeconomic, and infrastructure information). The features were standardized using z-score normalization (mean = 0, standard deviation = 1) prior to regression to ensure comparability of coefficients across features. We then fit linear regression models of the form

$$Y_S = \epsilon + \beta_0 + \sum_{i \in S} \beta_i X^{(i)} \tag{4}$$

using the *scikit-learn* module in Python and test their fitness by examining associated R-squared scores, similar to Equation (3).

Data availability

Original SafeGraph data are proprietary, and researchers can contact SafeGraph (<https://www.safegraph.com>). NAICS classifications are made available by the US Census (<https://www.census.gov/naics>). US Census data can be found at <https://data.census.gov>.

Code availability

Code base and processed network data can be found at https://github.com/NSF-ATD-MobilityNetwork/human_mobility.

Received: 28 August 2025; Accepted: 30 January 2026; Published online: 25 March 2026

References

- Gonzalez, M. C., Hidalgo, C. A. & Barabasi, A.-L. Understanding individual human mobility patterns. *Nature* **453**, 779–782 (2008).
- Louail, T. et al. Uncovering the spatial structure of mobility networks. *Nat. Commun.* **6**, 6007 (2015).
- Louf, R. & Barthelemy, M. How congestion shapes cities: from mobility patterns to scaling. *Sci. Rep.* **4**, 5561 (2014).
- Meloni, S. et al. Modeling human mobility responses to the large-scale spreading of infectious diseases. *Sci. Rep.* **1**, 62 (2011).
- Tizzoni, M. et al. On the use of human mobility proxies for modeling epidemics. *PLoS Comput. Biol.* **10**, e1003716 (2014).
- Nilforoshan, H. et al. Human mobility networks reveal increased segregation in large cities. *Nature* **624**, 586–592 (2023).
- Xu, F. et al. Using human mobility data to quantify experienced urban inequalities. *Nat. Hum. Behav.* **9**, 654–664 (2025).
- Mucha, P. J., Richardson, T., Macon, K., Porter, M. A. & Onnela, J.-P. Community structure in time-dependent, multiscale, and multiplex networks. *Science* **328**, 876–878 (2010).
- Kivela, M. et al. Multilayer networks. *J. Complex Netw.* **2**, 203–271 (2014).
- Bianconi, G. *Multilayer Networks: Structure and Function* (Oxford University Press, 2018).
- De Domenico, M., Solé-Ribalta, A., Gómez, S. & Arenas, A. Navigability of interconnected networks under random failures. *Proc. Natl. Acad. Sci. USA* **111**, 8351–8356 (2014).
- Taylor, D. et al. Topological data analysis of contagion maps for examining spreading processes on networks. *Nat. Commun.* **6**, 7723 (2015).
- Chodrow, P. S., Al-Awwad, Z., Jiang, S. & González, M. C. Demand and congestion in multiplex transportation networks. *PLoS ONE* **11**, e0161738 (2016).
- Cardillo, A. et al. Emergence of network features from multiplexity. *Sci. Rep.* **3**, 1344 (2013).
- Taylor, D., Porter, M. A. & Mucha, P. J. Tunable eigenvector-based centralities for multiplex and temporal networks. *Multiscale Model. Simul.* **19**, 113–147 (2021).
- Belyi, A. et al. Global multi-layer network of human mobility. *Int. J. Geogr. Inf. Sci.* **31**, 1381–1402 (2017).
- Barthélemy, M. Spatial networks. *Phys. Rep.* **499**, 1–101 (2011).
- SafeGraph Inc. Safegraph places and patterns data. <https://www.safegraph.com> (2021). Accessed via academic license; data used under SafeGraph terms.
- Gao, S., Rao, J., Kang, Y., Liang, Y. & Kruse, J. Mapping county-level mobility pattern changes in the United States in response to COVID-19. *SIGSpatial Spec.* **12**, 16–26 (2020).
- Coleman, N., Esmalian, A. & Mostafavi, A. Anatomy of susceptibility for shelter-in-place households facing infrastructure service disruptions caused by natural hazards. *Int. J. Disaster Risk Reduct.* **50**, 101875 (2020).
- Deng, H. et al. High-resolution human mobility data reveal race and wealth disparities in disaster evacuation patterns. *Humanit. Soc. Sci. Commun.* **8**, 1–8 (2021).
- Li, X., Qiang, Y. & Cervone, G. Using human mobility data to detect evacuation patterns in Hurricane Ian. *Ann. GIS* **30**, 493–511 (2024).
- Wang, Y., Wang, Q. & Taylor, J. E. Aggregated responses of human mobility to severe winter storms: an empirical study. *PLoS ONE* **12**, e0188734 (2017).
- Switek, P. Texas puts final estimate of winter storm death toll at 246. *The Texas Tribune* <https://www.texastribune.org/2022/01/02/texas-winter-storm-final-death-toll-246/>.
- McCullough, J. Texas’ final winter storm death toll is 246, a nearly doubling of the initial count. <https://www.texastribune.org/2022/01/>

- 02/texas-winter-storm-final-death-toll-246/. Accessed 21 April 2025 (2022).
26. McEntire, D. A. *Transportation and Logistics Problems During Winter Storm Uri*. Technical Report. https://ihsonline.org/Portals/0/Tech%20Papers/McEntire_Transportation_and_Logistics_Problems_Winter_Storm_Uri.pdf. Accessed 21 April 2025 (Institute for Homeland Security, 2021).
 27. Harris County Office of Homeland Security and Emergency Management. Update: Harris County urges residents to prepare for historic winter freeze. <https://www.readyharris.org/Newsroom/ReadyHarris-Alerts/All-Previous-Alerts/update-harris-county-urges-residents-to-prepare-for-historic-winter-freeze> Accessed 6 January 2026 (2021).
 28. Amanda Cochran, D. S. P. M. Closures, modified hours of businesses, venues across the Houston area. <https://www.click2houston.com/news/local/2021/02/15/beyond-schools-closures-modified-hours-across-the-houston-area-you-need-to-know-about-from-airports-to-grocery-stores/> Accessed 6 January 2026 (2021).
 29. Zhou, R. Z., Hu, Y., Zou, L., Cai, H. & Zhou, B. Understanding the disparate impacts of the 2021 Texas winter storm and power outages through mobile phone location data and nighttime light images. *Int. J. Disaster Risk Reduct.* **103**, 104339 (2024).
 30. Tiedmann, H. R. et al. Tracking the post-disaster evolution of water infrastructure resilience: a study of the 2021 Texas winter storm. *Sustain. Cities Soc.* **91**, 104417 (2023).
 31. Grineski, S. E. et al. Social disparities in the duration of power and piped water outages in Texas after winter storm Uri. *Am. J. Public Health* **113**, 30–34 (2023).
 32. Lee, C.-C., Maron, M. & Mostafavi, A. Community-scale big data reveals disparate impacts of the Texas winter storm of 2021 and its managed power outage. *Humanit. Soc. Sci. Commun.* **9**, 1–12 (2022).
 33. Chen, P., Zhai, W. & Yang, X. Enhancing resilience and mobility services for vulnerable groups facing extreme weather: lessons learned from snowstorm Uri in Harris County, Texas. *Nat. Hazards* **118**, 1573–1594 (2023).
 34. Song, C., Qu, Z., Blumm, N. & Barabási, A.-L. Limits of predictability in human mobility. *Science* **327**, 1018–1021 (2010).
 35. Yang, Y., Herrera, C., Eagle, N. & González, M. C. Limits of predictability in commuting flows in the absence of data for calibration. *Sci. Rep.* **4**, 5662 (2014).
 36. Cuttone, A., Lehmann, S. & González, M. C. Understanding predictability and exploration in human mobility. *EPJ Data Sci.* **7**, 2 (2018).
 37. Nejat, A., Solitare, L., Pettitt, E. & Mohsenian-Rad, H. Equitable community resilience: the case of winter storm Uri in Texas. *Int. J. Disaster Risk Reduct.* **77**, 103070 (2022).
 38. Xu, J., Qiang, Y., Cai, H. & Zou, L. Power outage and environmental justice in winter storm Uri: an analytical workflow based on nighttime light remote sensing. *Int. J. Digit. Earth* **16**, 2259–2278 (2023).
 39. Stanley, N., Shai, S., Taylor, D. & Mucha, P. J. Clustering network layers with the strata multilayer stochastic block model. *IEEE Trans. Netw. Sci. Eng.* **3**, 95–105 (2016).
 40. Caceres, R. S., Berger-Wolf, T. & Grossman, R. Temporal scale of processes in dynamic networks. In *Proc. 2011 IEEE 11th International Conference on Data Mining Workshops* 925–932 (IEEE, 2011).
 41. Taylor, D., Caceres, R. S. & Mucha, P. J. Super-resolution community detection for layer-aggregated multilayer networks. *Phys. Rev. X* **7**, 031056 (2017).
 42. Limón, E. Here’s how the COVID-19 pandemic has unfolded in Texas since March. <https://www.texastribune.org/2020/07/31/coronavirus-timeline-texas/>. Accessed 17 October 2025 (2020).
 43. Office of the Texas Governor. Governor’s strike force to open Texas. <https://open.texas.gov/> (2025).
 44. Li, Z., Ning, H., Jing, F. & Lessani, M. N. Understanding the bias of mobile location data across spatial scales and over time: a comprehensive analysis of safeGraph data in the United States. *PLoS ONE* **19**, e0294430 (2024).
 45. Chang, T., Hu, Y., Taylor, D. & Quigley, B. M. The role of alcohol outlet visits derived from mobile phone location data in enhancing domestic violence prediction at the neighborhood level. *Health Place* **73**, 102736 (2022).

Acknowledgements

This work is supported by the U.S. National Science Foundation under Grant No. DMS-2401276. Any opinions, findings, and conclusions or recommendations expressed in this material are those of the authors and do not necessarily reflect the views of the National Science Foundation. The authors also thank SafeGraph for providing anonymized mobile phone location data and the Jay Kemmer WORTH Institute for seed funding.

Author contributions

All authors developed the study and contributed regularly. M.B., A.K. and F.A. implemented the analyses. M.B. led the manuscript writing and figure development. All authors reviewed the manuscript.

Competing interests

The authors declare no competing interests.

Additional information

Supplementary information The online version contains supplementary material available at <https://doi.org/10.1038/s44260-026-00076-0>.

Correspondence and requests for materials should be addressed to Melissa Butler or Dane Taylor.

Reprints and permissions information is available at <http://www.nature.com/reprints>

Publisher’s note Springer Nature remains neutral with regard to jurisdictional claims in published maps and institutional affiliations.

Open Access This article is licensed under a Creative Commons Attribution 4.0 International License, which permits use, sharing, adaptation, distribution and reproduction in any medium or format, as long as you give appropriate credit to the original author(s) and the source, provide a link to the Creative Commons licence, and indicate if changes were made. The images or other third party material in this article are included in the article’s Creative Commons licence, unless indicated otherwise in a credit line to the material. If material is not included in the article’s Creative Commons licence and your intended use is not permitted by statutory regulation or exceeds the permitted use, you will need to obtain permission directly from the copyright holder. To view a copy of this licence, visit <http://creativecommons.org/licenses/by/4.0/>.

© The Author(s) 2026